GEOLOGY | THE GEOLOGICAL SOCIETY OF AMERICA®

https://doi.org/10.1130/G48114.1

Manuscript received 8 July 2020
Revised manuscript received 29 August 2020
Manuscript accepted 25 September 2020

Characterizing strain between rigid crustal blocks in the southern Cascadia forearc: Quaternary faults and folds of the northern Sacramento Valley, California

Stephen Angster[1]*, Steven Wesnousky[1], Paula Figueiredo[2], Lewis A. Owen[2] and Thomas Sawyer[3]
[1]Center for Neotectonic Studies, University of Nevada–Reno, Reno, Nevada 89557, USA
[2]Department of Marine, Earth, and Atmospheric Sciences, North Carolina State University, Raleigh, North Carolina 27695, USA
[3]Piedmont GeoSciences, Inc., HC72 Box 20233, Dyer, Nevada 89010, USA

ABSTRACT

Topographic profiles across late Quaternary surfaces in the northern Sacramento Valley (California, USA) show offset and progressive folding on series of active east- and northeast-trending faults and folds. Optically stimulated luminescence ages on deposits draping a warped late Pleistocene river terrace yielded differential incision rates along the Sacramento River and indicate tectonic uplift equal to 0.2 ± 0.1 and 0.6 ± 0.2 mm/yr above the anticline of the Inks Creek fold system and Red Bluff fault, respectively. Uplift rates correspond to a total of 1.3 ± 0.4 mm/yr of north-directed crustal shortening, accounting for all of the geodetically observed contractional strain in the northern Sacramento Valley, but only part of the far-field contraction between the Sierra Nevada–Great Valley and Oregon Coast blocks. These structures define the southern limit of the transpressional transition between the two blocks.

INTRODUCTION

Differential motion between the more rapidly northwest-translating Sierra Nevada–Great Valley (SNGV) block and slower clockwise-rotating Oregon Coast (OC) block (Argus and Gordon, 1991, 2001; Wells et al., 1998; Wells and Simpson, 2001; Humphreys and Coblentz, 2007; McCaffrey et al., 2013) predicts north-south contraction and dextral shear deformation across the southern Cascadia forearc (Fig. 1; Hammond and Thatcher, 2005; Unruh and Humphrey, 2017). The northern Sacramento Valley lies within this boundary zone, where previously mapped structures oriented to accommodate such contraction include the (1) Red Bluff fault, (2) Inks Creek fold system (ICFS)/Hooker Dome, (3) Battle Creek fault, and (4) Bear Creek fault (Fig. 1; Helley et al., 1981; Blake et al., 1999). These east- and northeast-trending faults and folds define the Battle Creek structural domain (Harwood and Helley, 1987) and are generally perpendicular to localized contemporary strain shortening axes delineated from seismology (Fig. 1; Unruh and Humphrey, 2017).

We mapped, analyzed, and dated late Quaternary deposits and river terraces along an ~100-km-long stretch of the Sacramento River channel from the city of Redding to south of Red Bluff, California (Fig. 2A), to document the recency, style, and rate of crustal deformation associated with the mapped faults and folds using standard field mapping, lidar data, and optically stimulated luminescence (OSL) geochronology. Our observations formed the basis for quantifying the rates of deformation on individual structures, estimating the rate of late Quaternary north-south shortening across the region, and discussing the kinematics by which contemporary strain between the rigid intraplate SNGV and OC blocks is accommodated.

LATE CENOZOIC DEFORMATION IN THE NORTHERN SACRAMENTO VALLEY

Structures of the Battle Creek domain represent the youngest phase of northward-propagating late Cenozoic deformation in the Sacramento Valley, correlative to migration of the Mendocino triple junction (Fig. 1; Harwood and Helley, 1987). Interpretations of seismic reflection profiles (Fig. S1 in the Supplemental Material[1]; Harlan Miller Tait, 1984) and prior mapping (Helley et al., 1981; Blake et al., 1999) depict the Battle Creek fault as a steeply south-dipping Cretaceous normal fault that offsets late Quaternary deposits at the surface. A secondary component of right-lateral slip is inferred on the Battle Creek fault from mapped fracture patterns (Helley et al., 1981), which is consistent with the orientation of localized contemporary strain shortening axes (Fig. 1). To the south, Pliocene strata are folded at the surface by steeply dipping blind reverse faults below the ICFS and the low-angle north-dipping blind Red Bluff fault (Fig. S1; Harwood, 1984).

The style and kinematics of mid- to late Quaternary deformation across the east- and northeast-trending structures are illustrated by the topographic structural profile A-A′ in Figure 2B. The profile in Figure 2A traverses the coarse gravel deposits of the Red Bluff Formation (Qrb; <5 m thick; 1.08–0.4 Ma; Diller, 1906; Helley and Jaworowski, 1985) and a locally underlying thin (<10 m) undated Pleistocene basalt mapped as the Coleman Forebay basalt (Qcb; Blake et al., 1999). Both formations lie unconformably over Pliocene bedrock and form the highest geomorphic surfaces proximal to the Sacramento River channel (Fig. 2A). Late Quaternary down-to-the-south displacement, northward backtilting, and truncation of Qrb are manifested by the south-facing scarps of the Bear Creek and Battle Creek faults (Fig. 2B). Helley et al. (1981) measured 127 and 330–440 m of vertical separation of the base of Qrb and Qcb across the Battle Creek fault, respectively, yielding a

*Current address: U.S. Geological Survey, Seattle, Washington 98195, USA

[1]Supplemental Material. Supplemental figures and information about datasets and methods used for mapping and terrace profiling, and OSL dating methods, results, and discussion. Please visit https://doi.org/10.1130/GEOL.S.13182989 to access the supplemental material, and contact editing@geosociety.org with any questions.

CITATION: Angster, S., et al., 2020, Characterizing strain between rigid crustal blocks in the southern Cascadia forearc: Quaternary faults and folds of the northern Sacramento Valley, California: Geology, v. 49, p. , https://doi.org/10.1130/G48114.1

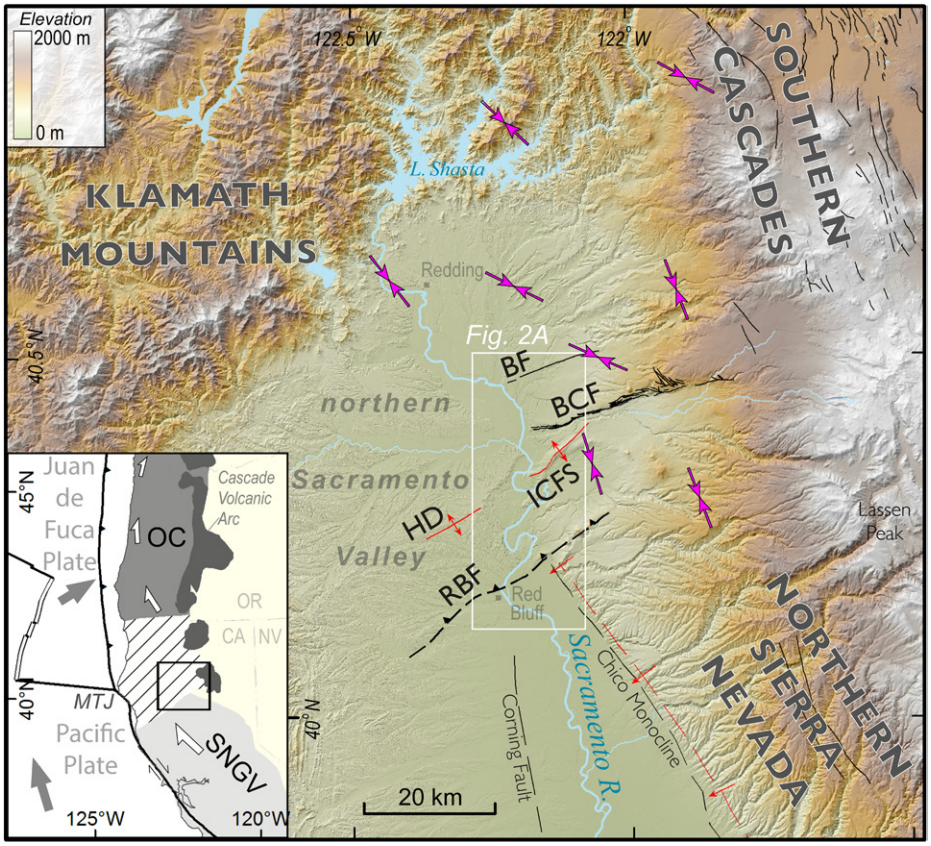

Figure 1. Mapped faults and folds in northern Sacramento Valley (Blake et al., 1999). RBF—Red Bluff fault, ICFS—Inks Creek fold system, HD—Hooker Dome, BCF—Battle Creek fault, BF—Bear Creek fault. Horizontal shortening strain axes (magenta arrows) are from Unruh and Humphrey (2017). Inset: Tectonic overview of rigid block motions (SNGV—Sierra Nevada–Great Valley block; OC—Oregon Coast block; MTJ—Mendocino triple junction). Hatched area shows region of geodetically observed north-south contraction (Williams et al., 2006; Hammond and Thatcher, 2005). OR—Oregon; CA—California; NV—Nevada.

late Quaternary vertical slip rate of <0.3 mm/yr. To the south, the discontinuous surface of Qcb arches over the folded Pliocene cored anticlinal ridge of the ICFS and again gradually rises southward from Table Mountain toward the Red Bluff fault and defines the Red Bluff anticline (Fig. 2B). We interpret the gently folded geometry of the basalt surface to reflect south-vergent folding above a blind north-dipping reverse fault within the ICFS and of the Red Bluff thrust fault (Fig. 2B).

SACRAMENTO RIVER GEOMORPHOLOGY AND TERRACE PROFILES

A sequence of abandoned Quaternary river terraces displays large meanders along the Sacramento River where it traverses structures of the Battle Creek domain (Fig. 2). We mapped and constructed profiles from lidar along four distinct terrace sets (T1–T4), described in the Supplemental Material, to observe potential deformation of the terrace surfaces. At the northern end of the map area (Fig. 2A), terraces T1–T4 are generally fill terraces that form broad expansive surfaces and show no discernible deformation within the longitudinal profiles that coincide with the mapped locations of the Bear Creek and Battle Creek faults (Fig. 3A). The lack of any apparent young displacement across these faults is consistent with the wide channel and expansive spatial distribution of the terraces at this point along the river (Fig. 2A; e.g., Amos and Burbank, 2007). The T3 terrace profile displays a slight fall in relative elevation to the modern Sacramento River (Fig. 3A), suggesting post-T3 down-to-S slip on the Battle Creek fault or downwarp associated with the ICFS.

Evidence of uplift is observed where the Sacramento River enters the more incised, narrow, and sinuous channel beginning at the ICFS (Fig. 2A). The emergence of fresh bedrock straths in the modern channel, strath terraces (T1–T4) that are progressively blanketed by overbank deposits, and a wind and water gap (Fig. 2C) indicate progressive westward propagation and uplift of the ICFS anticlinal ridge (e.g., Bullard and Lettis, 1993). T3 and T4 show a rise in relative height above the modern river at ~39 km river distance (Fig. 3A), and then again at ~57 km river distance (Fig. 3A). The younger T2 and T3 show a similar rise, but to a progressively lesser degree farther downstream at ~64 km river distance (Fig. 3A). The point at which the terrace surfaces are the highest relative to the river (~73 km river distance) coincides with Iron Canyon, the deepest section of the river channel where terrace preservation is least, and this marks the location where we define the axis to the Red Bluff anticlinal fold above the Red Bluff fault (Figs. 2D and 3A). By matching the location of this axis with the anticlinal axis defined by the deformed Qcb in the topographic profile over the Red Bluff fault (Fig. 2B), we delineated the axial trend of the Red Bluff anticline, which generally trends parallel to the Red Bluff fault (Fig. 2A). Downstream of the Red Bluff fault, the river channel widens, and the river terraces are more widespread and become fill terraces as the terrace treads once again approach parallel to the modern river grade (Figs. 2A and 3A).

We interpreted two zones of tectonic uplift where terrace profiles deviate from the slope of the Sacramento River (Fig. 3A). In general, the geometry of the warped T3 and T4 surfaces across the ICFS and above the Red Bluff fault reflects the same general asymmetric geometry as that evident in the Qcb (Fig. 3A), indicating progressive late Quaternary folding above the Red Bluff fault and ICFS anticline. Terrace surfaces are in contrast undeformed across the Bear Creek fault and only slightly offset across the Battle Creek fault, suggesting little to no recent vertical motion on these faults during the late Quaternary.

RIVER INCISION AND UPLIFT RATES

We calculated fluvial incision rates along the Sacramento River using the T3 terrace, the most continuous and most exposed warped river terrace, by dividing the relative height of the T3 terrace treads above the modern river by the OSL age of samples collected from T3 deposits (Fig. 2A). Details and photographs of OSL samples are presented in Figures S3–S6 and Table S1. The OSL age results indicate a maximum age of T3 surface abandonment at 27.7 ± 9.3 ka (see the Supplemental Material for a discussion), and so the following rates should be considered as minimum values. Based on these results, we determined differential late Quaternary fluvial incision rates along the studied section of river, with the highest rate (1.1 ± 0.3 mm/yr) occurring within Iron Canyon (Fig. 3B), where we delineated the Red Bluff anticline axis over the Red Bluff fault (Fig. 2D). The lowest rates of incision occur immediately downstream of the Red Bluff fault and average ~0.5 mm/yr (Fig. 3B). Rates of incision through the ICFS reach up to 0.9 ± 0.2 mm/yr within the hinge zone of the anticline and drop to 0.7 ± 0.2 mm/yr within the syncline to the south

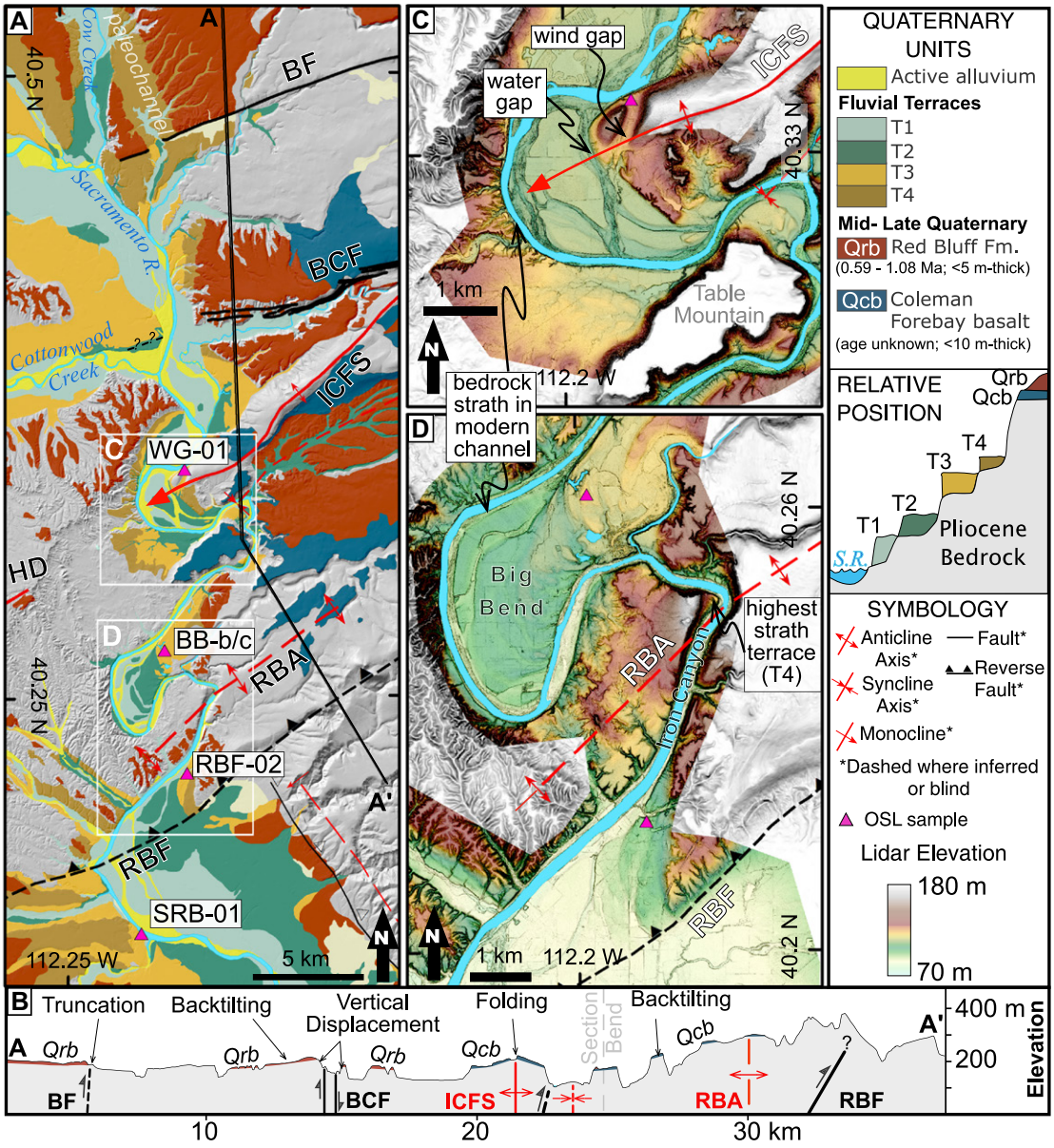

Figure 2. (A) Map of Quaternary units, mapped structures (see Fig. 1 caption; RBA—Red Bluff anticline), and sample locations along the studied section of the Sacramento River (S.R.), California, USA. (B) Topographic profile A-A′ extracted from 10 m digital elevation model. (C–D) Lidar elevation maps of (C) Inks Creek fold system (ICFS) and (D) Red Bluff anticline and fault. OSL—optically stimulated luminescence.

(Fig. 3B). Although uplift was not evident in the profiles upstream from the ICFS, incision rates are elevated, averaging ~0.9 mm/yr (Fig. 3B). This may reflect broad-scale uplift associated with late Quaternary slip on the Battle Creek fault zone and Bear Creek fault; however, this broader pattern of uplift is not reflected within the older Qrb, and so we instead interpreted this to indicate near-fault deformation across these faults (Fig. 2B). We suspect the higher rate may be reflecting the natural incision rate of the river in the upper valley, where the river has a steeper gradient and where Quaternary and Pliocene alluvial deposits are thicker (Blake et al., 1999), and thus easier for the river to incise (e.g., Lavé and Avouac, 2001). Alternatively, this could reflect long-wavelength uplift of the Klamath Mountains (Fig. 1); however, modern topography and geodesy indicate that uplift is mostly confined within the Klamath Mountains (Hammond et al., 2016).

To estimate the differential incision rate due to tectonic uplift across the anticlines, we assumed that deformation has only occurred within the two zones of uplift documented in the T3 deposits (Fig. 3A). Thus, the gradients of the T3 surface above and below these two uplift zones should reflect the original gradient of the river at the time of T3 abandonment (27.7 ± 9.3 ka). Assuming this is true, we determined a best-fit curve of the former river during T3 abandonment by applying a convex exponential curve using T3 elevation points on either side of the zones of uplift (dashed orange line in Fig. 3A). By measuring the height differences between the projected T3 former river gradient and the highest T3 surface points within the uplift zones above the ICFS anticline (4.8 ± 0.5 m) and Red Bluff anticline (14 ± 0.5 m), respectively, and dividing these values by the T3 abandonment age (27.7 ± 9.3 ka), we calculated uplift rates of 0.2 ± 0.1 and 0.6 ± 0.2 mm/yr, respectively (Fig. 3B).

We computed shortening rates based on the simple geometric relationship between the tectonic uplift rate and an assumed master 30° thrust fault for the Red Bluff fault and 45° reverse fault for the ICFS anticline based on the general subsurface geometries (Fig. S1) and applying Andersonian fault mechanics (Anderson, 1951). This first-order approach estimates late Quaternary horizontal shortening rates of 0.2 ± 0.1 and 1.1 ± 0.3 mm/yr on a reverse fault beneath the ICFS anticline and the Red Bluff thrust fault, respectively. Due to the relatively low dip angles assumed in these estimations, these rates should be considered as maximum values.

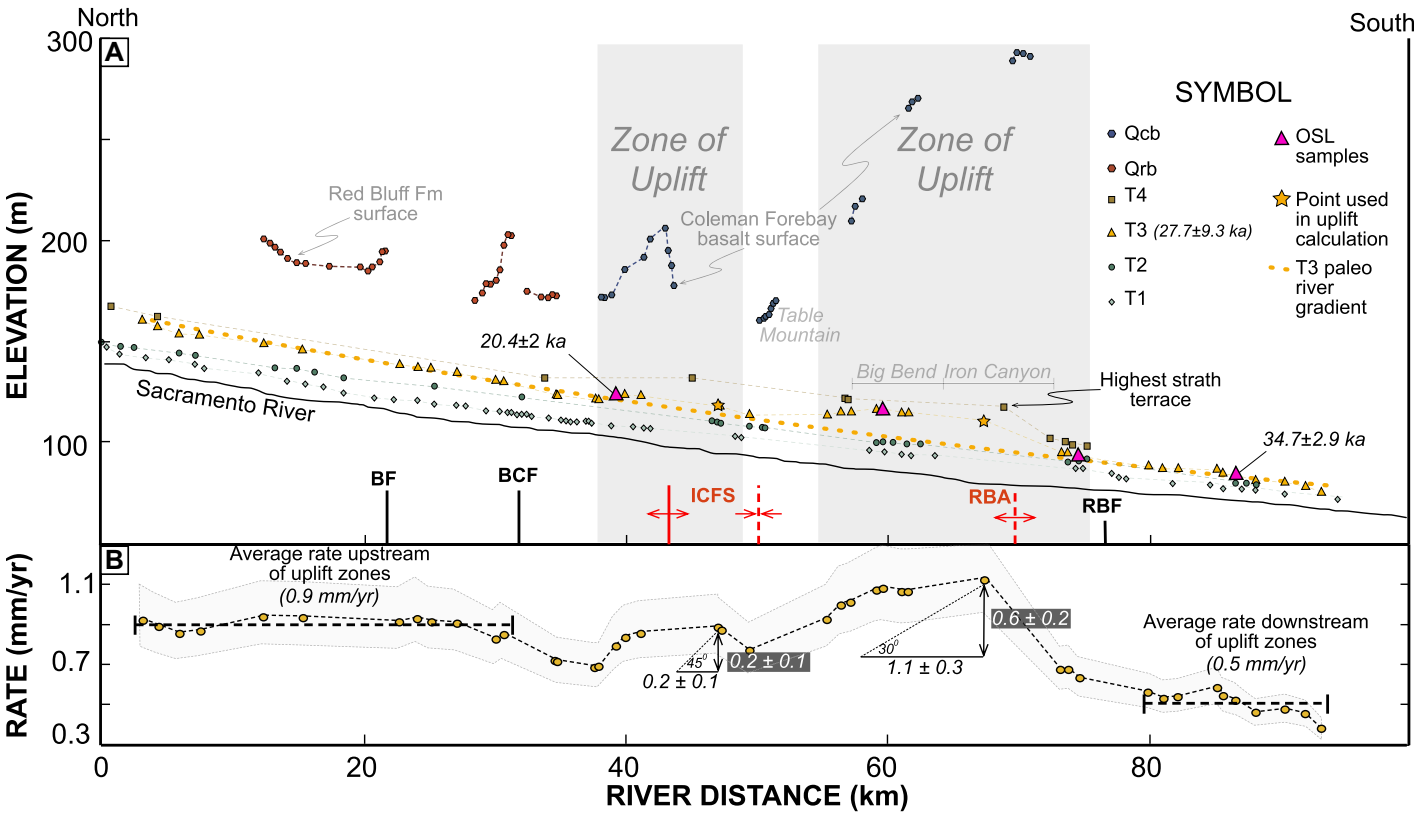

Figure 3. (A) Longitudinal profiles of mapped river terraces and late Quaternary deposits along the Sacramento River, California, USA (see captions for Figs. 1 and 2 for abbreviations; see the Supplemental Material [see footnote 1] for methods). Terrace T3 former river gradient (orange dash line) was determined from best-fit exponential curve using T3 elevation points on either side of zones of uplift (gray shading). (B) Terrace incision rate with uncertainty (shading) based on T3 surface and optically stimulated luminescence (OSL) ages. Rates with black background are tectonic uplift rate estimates (mm/yr).

DISCUSSION AND CONCLUSIONS

The topographic profiles across the late Quaternary deposits show that late Quaternary folding across the blind Red Bluff fault and, to a lesser degree, the ICFS accommodates contemporary north-south contraction in the northern Sacramento Valley, whereby progressive lateral and vertical fold growth has deflected the Sacramento River to produce the large meanders and deformed terrace surfaces. While the cumulative late Pleistocene shortening rate across these structures equals 1.3 ± 0.4 mm/yr, matching the geodetically observed ~1 mm/yr of north-south contraction reported across the northern Sacramento Valley (Unruh and Humphrey, 2017), up to 4 mm/yr of contraction is observed in the far-field region across northern California and southern Oregon (Hammond and Thatcher, 2005). Thus, the boundary between the SNGV and OC blocks is not confined to the Sacramento Valley. The abrupt change in strike of the northeast-striking Red Bluff fault against the north-south–striking structures to the south (Fig. 1) suggests it to be the southernmost structural boundary between the SNGV and OC blocks (Fig. 4). Other boundary-accommodating structures likely exist to the north within the geodetically observed zone of transpression that divides the SNGV and OC blocks (Fig. 4).

Northwest translation of the SNGV block drives large-scale northwest-directed transtensional dextral shear deformation east of the Sierra Nevada (e.g., Unruh et al., 2003) and in the Cascadia backarc (e.g., Langenheim et al., 2015; Waldien et al., 2019), a portion of which extends westward between and south of the volcanic centers of the southern Cascade arc (Fig. 4; Blakely et al., 1997). Accommodation of this dextral strain across the southern Cascadia forearc (~5 mm/yr; Unruh and Humphrey, 2017) remains enigmatic. The suggestion of right-lateral slip on the Battle Creek fault and Bear Creek fault (Helley et al., 1981) seems plausible when considering their relative orientations to localized contemporary strain shortening axes determined from seismology (Fig. 1; Unruh and Humphrey, 2017). These faults exhibit evidence for longer-term vertical slip, but we found no evidence within the Sacramento River channel for horizontal offset. The high effective stream power of the Sacramento River may account for the lack of preservation of horizontal offset (e.g., Larsen et al., 2006). In this sense, some degree of dextral slip could be expected on the subparallel Bear Creek and Battle Creek faults, thus characterizing the Battle Creek structural domain as an active transpressional fault system. The long-lived slip history on the Battle Creek fault suggests that preexisting structure may influence the kinematics on this fault and possibly on the Bear Creek fault (Magill and Cox, 1981). Northwest of the SNGV block, reverse and dextral strike-slip faults are reported to also accommodate north-south shortening (Fig. 4; Williams et al., 2006). Combining these observations with ours defines a southern limit to a diffuse transpressional boundary between the rigid SNGV and OC blocks (Fig. 4).

While geodesy often tells us that there are discrete rigid blocks with boundaries within broad plate boundaries, the nature of deformation at these block boundaries remains intractable without dense field arrays. Even with such arrays, the long-term deformation rates cannot be determined. This study shows that detailed field work at such boundaries can extract subtle tectonic signals of long-term progressive deformation on discrete structures, enabling better locations and characterization of potential seismically active sources in intraplate settings.

ACKNOWLEDGMENTS

Much credit is given to David Harwood and Edward Helley for their early recognition and understanding of these structures. Thoughtful reviews by Austin Elliot, Vicki Langenheim, Bill Hammond, Colin Amos, and Harvey Kelsey greatly improved the quality of this manuscript. Brian Sherrod provided

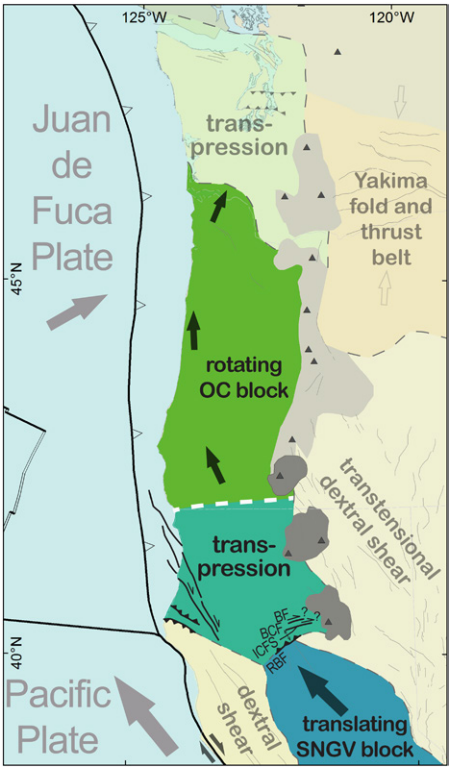

Figure 4. Modified tectonic model of Wells and Simpson (2001) with active faults (black lines) accommodating transpressional strain between the Sierra Nevada–Great Valley (SNGV) and Oregon Coast (OC) blocks (see Fig. 1 caption). Light-gray lines show other active faults. Dark-gray areas show volcanic centers (Blakely et al., 1997). White dashed line shows northern limit of north-south geodetic contraction from Hammond and Thatcher (2005).

useful comments during the preparation of this manuscript. The California Department of Water Resources provided the lidar data. Research was supported in part by National Science Foundation grants EAR-1345036 and EAR-1419724. This is Center for Neotectonics Studies (University of Nevada at Reno) contribution 81.

REFERENCES CITED

Amos, C.B., and Burbank, D.W., 2007, Channel width response to differential uplift: Journal of Geophysical Research–Earth Surface, v. 112, F02010, https://doi.org/10.1029/2006JF000672.

Anderson, E.M., 1951, Dynamics of Faulting and Dyke Formations with Application to Britain: Edinburgh, UK, Oliver & Boy, 191 p.

Argus, D.F., and Gordon, R.G., 1991, Current Sierra Nevada–North America motion from very long baseline interferometry: Implications for the kinematics of the western United States: Geology, v. 19, p. 1085–1088, https://doi.org/10.1130/0091-7613(1991)019<1085:CSNNAM>2.3.CO;2.

Argus, D.F., and Gordon, R.G., 2001, Present tectonic motion across the Coast Ranges and San Andreas fault system in central California: Geological Society of America Bulletin, v. 113, p. 1580–1592, https://doi.org/10.1130/0016-7606(2001)113<1580:PTMATC>2.0.CO;2.

Blake, M.C., Harwood, D.S., Helley, E.J., Irwin, W.P., and Jayko, A.S., 1999, Geologic Map of the Red Bluff 30′ × 60′ Quadrangle, California: U.S. Geological Survey Geologic Investigation Series Map I-2542, scale 1:100,000, https://pubs.usgs.gov/imap/2542/.

Blakely, R.J., Christiansen, R.L., Guffanti, M., Wells, R.E., Donnelly-Nolan, J.M., Muffler, L.P., Clynne, M.A., and Smith, J.G., 1997, Gravity anomalies, Quaternary vents, and Quaternary faults in the southern Cascade Range, Oregon and California: Implications for arc and backarc evolution: Journal of Geophysical Research: Solid Earth, v. 102, B10, p. 22513–22527, https://doi.org/10.1029/97JB01516.

Bullard, T.F., and Lettis, W.R., 1993, Quaternary fold deformation associated with blind thrust faulting, Los Angeles Basin, California: Journal of Geophysical Research, v. 98, B5, p. 8349–8369, https://doi.org/10.1029/93JB00012.

Diller, J.S., 1906, Redding Folio, California: U.S. Geological Survey Geologic Atlas of the United States Folio GF-138, scale 1:125,000, https://doi.org/10.3133/gf138.

Hammond, W.C., and Thatcher, W., 2005, Northwest Basin and Range tectonic deformation observed with the Global Positioning System, 1999–2003: Journal of Geophysical Research, v. 110, B10405, https://doi.org/10.1029/2005JB003678.

Hammond, W.C., Blewitt, G., and Kreemer, C., 2016, GPS imaging of vertical land motion in California and Nevada: Implications for Sierra Nevada uplift: Journal of Geophysical Research: Solid Earth, v. 121, p. 7681–7703, https://doi.org/10.1002/2016JB013458.

Harlan Miller Tait, 1984, Report of Fault Evaluation of the Cottonwood Creek Project for U.S. Army Corps of Engineers Sacramento District: Healdsburg, California, Harlan Miller Tait, Earth Sciences Associates, and Photographic Interpretation Corporation, 1983, Contract No. DACW05–82-C-0074.

Harwood, D.S., 1984, Evidence for late Cenozoic east-west compressive tectonism in the Sacramento Valley, California, *in* Crouch, J.K., and Bachman, S.B., eds., Tectonics and Sedimentation Along the California Margin: Pacific Section, Society of Economic Paleontologists and Mineralogists (SEPM), Book 38, p. 87–100.

Harwood, D.S., and Helley, E.J., 1987, Late Cenozoic Tectonism of the Sacramento Valley, California: U.S. Geological Survey Professional Paper 1359, 46 p., https://doi.org/10.3133/pp1359.

Helley, E.J., and Jaworowski, C., 1985, The Red Bluff Pediment—A Datum Plane for Locating Quaternary Structures in the Sacramento Valley, California: U.S. Geological Survey Bulletin 1628, 24 p.

Helley, E.J., Harwood, D.S., Barker, J.A., and Griffen, E.A., 1981, Geologic Map of the Battle Creek Fault Zone and Adjacent Parts of the Northern Sacramento Valley, California: U.S. Geological Survey Miscellaneous Field Studies Map MF-1298, scale 1:62,500, https://doi.org/10.3133/mf1298.

Humphreys, E.D., and Coblentz, D.D., 2007, North American dynamics and western U.S. tectonics: Reviews of Geophysics, v. 45, p. 1–30, https://doi.org/10.1029/2005RG000181.

Langenheim, V.E., Jachens, R.C., Muffler, L.J.P., and Clynne, M.A., 2015, Implications for the structure of the Hat Creek fault and transfer of right-lateral shear from the Walker Lane north of Lassen Peak, northern California, from gravity and magnetic data: Geosphere, v. 12, p. 790–808, https://doi.org/10.1130/GES01253.1.

Larsen, E.W., Premier, A.K., and Greco, S.E., 2006, Cumulative effective stream power and bank erosion on the Sacramento River, California, USA: Journal of the American Water Resources Association, v. 42, p. 1077–1097, https://doi.org/10.1111/j.1752-1688.2006.tb04515.x.

Lavé, J., and Avouac, J.P., 2001, Fluvial incision and tectonic uplift across the Himalayas of central Nepal: Journal of Geophysical Research, v. 105, p. 5735–5770, https://doi.org/10.1029/1999JB900292.

Magill, J., and Cox, A., 1981, Post-Oligocene tectonic rotation of the Oregon western Cascade Range and the Klamath Mountains: Geology, v. 9, p. 127–131, https://doi.org/10.1130/0091-7613(1981)9<127:PTROTO>2.0.CO;2.

McCaffrey, R., King, R.W., Payne, S.J., and Lancaster, M., 2013, Active tectonics of northwestern U.S. inferred from GPS-derived surface velocities: Journal of Geophysical Research: Solid Earth, v. 118, p. 709–723, https://doi.org/10.1029/2012JB009473.

Unruh, J., and Humphrey, J., 2017, Seismogenic deformation between the Sierran microplate and Oregon Coast block, California, USA: Geology, v. 45, p. 415–418, https://doi.org/10.1130/G38696.1.

Unruh, J., Humphrey, J., and Barron, A., 2003, Transtensional model for the Sierra Nevada frontal fault system, eastern California: Geology, v. 31, p. 327–330, https://doi.org/10.1130/0091-7613(2003)031<0327:TMFTSN>2.0.CO;2.

Waldien, T.S., Meigs, A.J., and Madin, I.P., 2019, Active dextral strike-slip faulting records termination of the Walker Lane belt at the southern Cascade arc in the Klamath graben, Oregon, USA: Geosphere, v. 15, p. 882–900, https://doi.org/10.1130/GES02043.1.

Wells, R.E., and Simpson, R.W., 2001, Northward migration of the Cascadia forearc in the northwestern U.S. and implications for subduction deformation: Earth, Planets, and Space, v. 53, p. 275–283, https://doi.org/10.1186/BF03352384.

Wells, R.E., Weaver, C.S., and Blakely, R.J., 1998, Fore-arc migration in Cascadia and its neotectonic significance: Geology, v. 26, p. 759–762, https://doi.org/10.1130/0091-7613(1998)026<0759:FAMICA>2.3.CO;2.

Williams, T.B., Kelsey, H.M., and Freymueller, J.T., 2006, GPS-derived strain in northwestern California: Termination of the San Andreas fault system and convergence of the Sierra Nevada–Great Valley block contribute to southern Cascadia forearc contraction: Tectonophysics, v. 413, p. 171–184, https://doi.org/10.1016/j.tecto.2005.10.047.

Printed in USA